MAGNETIC RESONANCE IN CHEMISTRY, VOL. 35, 619–628 (1997)

Novel Model Compounds for Photoinduced Electron Transfer: Structures of the Folded Conformers of Zinc(II)–Pyropheophytin–Anthraquinone Dyads

Juho Helaja,[1,2] Andrei Y. Tauber,[1] Ilkka Kilpeläinen[2] and Paavo H. Hynninen[1]*
[1] Department of Chemistry, University of Helsinki, P.O. Box 55, FIN-00014 University of Helsinki, Finland
[2] Institute of Biotechnology, University of Helsinki, P.O. Box 56, FIN-00014 University of Helsinki, Finland

The solution structures of the P4-epimers of Zn(II)–pyropheophytin–anthraquinone dyads (ZnPQ1 and ZnPQ2) were determined using two-dimensional NMR spectroscopy and molecular modeling. The mutual orientation of the anthraquinone and Zn–pyropheophytin rings was found to be different in the two P4-epimeric dyads on the basis of the ROESY correlations, observed between the quinone and phorbin protons. The anthraquinone ring is situated below the phorbin macrocycle in both dyads, ZnPQ1 and ZnPQ2. In ZnPQ1, the ring planes show tilting, the anthraquinone ring being in a sloping position below subrings B, C and E of the phorbin macrocycle. In ZnPQ2, the two π-systems are almost parallel with the anthraquinone ring being located approximately below the center of the phorbin macrocycle. © **1997 by John Wiley & Sons, Ltd.**

Magn. Reson. Chem. **35**, 619–628 (1997) No. of Figures: 6 No. of Tables: 3 No. of References: 32

Keywords: NMR; ^{1}H NMR; ^{13}C NMR; ROESY; spin simulation; pheophytin; anthraquinone

Received 7 January 1997; accepted 14 April 1997

INTRODUCTION

The covalently linked Zn(II)–pyropheophytin–anthraquinone dyads (Fig. 1) have been used as donor–acceptor systems in photo-induced electron transfer studies.[1] The mutual distances and orientations of the donor and acceptor are important for understanding the kinetics and mechanisms of electron transfer in these systems. On the basis of photochemical[1] and NMR studies[2] of the metal-free molecules H_2PQ1 and H_2PQ2, it has been found that, in solution, there are two main types of conformers, the folded ones and the opened ones, in fast equilibrium with one another. The folded ones have been proposed to be the dominating conformers in chloroform and acetonitrile.[2]

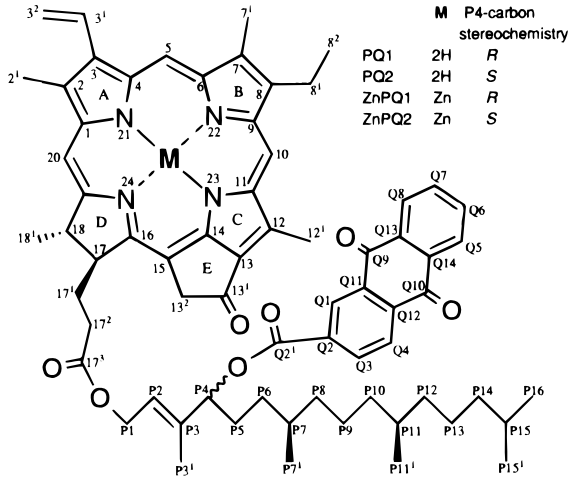

Figure 1. Structures and numbering of the covalently linked pyropheophytin–anthraquinone dyads. Also given are the abbreviations used for the compounds and the stereochemical configuration at carbon P4.

In the former investigations of porphyrin–quinone dyads covalently linked at a *meso* position of the porphyrin by a short spacer group, only the presence of open conformers could be observed in solution.[3] However, in the studies on pheophorbide–quinone dyads, evidence for the formation of folded conformers was obtained by ^{1}H NMR.[4] Also, the ^{1}H NMR $\Delta\delta$ values concerning the metal-free pyropheophytin–anthraquinone dyads, covalently linked by a flexible spacer group, showed clear evidence of the existence of folded conformers.[2]

Zn(II) in porphyrins and pheophorbides is known to be strictly five-coordinated even in presence of an excess of ligand.[5–7] In the case of ZnPQ molecules, the fifth ligand can be intramolecularly one of the anthraquinone carbonyl oxygens. The existence of folded conformers for the sulfonyloxy-bridged Zn(II)–porphyrin–anthraquinone dyads has been observed earlier in $CDCl_3$.[8] The presence of the folded conformers was judged from $\Delta\delta_H$ values observed for the anthraquinonyl protons. The coordination of the anthraquinonyl carbonyl oxygen to the central zinc atom was suggested as a mechanism for the folding.[8]

* *Correspondence to*: P. H. Hynninen.

 CCC 0749–1581/97/090619–10 $17.50

Previously, ^{1}H NMR $\Delta\delta$ values have been used to construct models for pheophytin aggregates.[9–12] In the pheophytin dimers, changes in the δ_H values ($\Delta\delta_H$) arise from dissimilar ring-current effects in the monomer and dimer structures. On the basis of ring-current effects,[13,14] the $\Delta\delta_H$ values are expected to be largest for the overlapped area of the two π-systems in a parallel orientation. Attractive π–π interactions are known to afford a driving force determining the geometry between aromatic systems.[15] The nature of π–π interactions has been considered predominantly between two similar molecules, e.g. between porphyrins. In the porphyrins studied, the intermolecular interaction between the molecules is strongest when the macrocycles are in a slipped, parallel orientation. Strong π–π interaction between porphyrin molecules often causes self-aggregation. Zn metallation has been observed to increase π–π interactions in the case of some porphyrins.[15]

Modern NMR techniques offer an efficient way to analyze solution structures of chlorophyll compounds.[16–18] Heteronuclear multiple quantum coherence (HMQC) and heteronuclear multiple quantum multiple bond coherence (HMBC) experiments[19] can be used to obtain the complete ^{1}H and ^{13}C assignments for these compound.[16,17] 2D ROESY[20] can be used to obtain stereochemical information about the closely spaced proton-bearing groups.[18]

In this paper, we show that by combining the information obtained from ROESY with that from the ^{1}H NMR $\Delta\delta$ values, it is possible to deduce the relative orientation between the phorbin and anthraquinone rings in ZnPQ1 and ZnPQ2. Further, we will show that the conformational analysis of the propionic ester side chain[21–23] and the front part of the phytyl chain[23,24] can be executed utilizing ^{1}H NMR spectral simulation and rotamer population analysis. The conformation of ring D can be determined from the vicinal coupling between the 17-CH and 18-CH protons using the simple Karplus equation.[25,26] Finally, we will demonstrate that on the basis of the structural information obtained by the above NMR experiments, reasonable molecular models for ZnPQ1 and ZnPQ2 can be constructed.

RESULTS AND DISCUSSION

Assignment of the ^{1}H and ^{13}C NMR spectra

The assignments of the ^{1}H and ^{13}C NMR spectra of 9,10-anthracenedione-2-carboxylic acid methyl ester (Q), Zn(II)–13^2-(demethoxycarbonyl)pheophytin *a* (ZnP) and Zn(II)–13^2-demethoxycarbonyl-P4(*R*,*S*)-oxy-(9,10-anthracenedione-2-carbonyl)pheophytin *a* (ZnPQ1 and ZnPQ2) are presented in the Experimental section. Complete ^{1}H and ^{13}C assignments for ZnP, ZnPQ1 and ZnPQ2 were obtained except for the phytyl residue (P5–P16) using HMQC and HMBC experiments in concert.[16] Although the ZnPQ1 and ZnPQ2 molecules differ only in the stereochemistry of carbon P4,[2] clear differences were observed in the chemical shifts of the ^{1}H and ^{13}C NMR spectra. These can be attributed to the differences in the interplanar ring-current effects, arising from the different relative positions of the anthraquinone and phorbin rings in ZnPQ1 and ZnPQ2.

The ^{1}H and ^{13}C NMR spectra of Q and the anthraquinone part of ZnPQ1 and ZnPQ2 molecules (Fig. 1) were assigned as follows. First, the Q1-CH proton was identified as a doublet, resulting from the coupling over four bonds to Q3-CH. A doublet of doublets was observed for Q3-CH, because it was also coupled to proton Q4-CH. Then, the anthraquinone Q8-CH and Q5-CH protons were assigned from their HMBC correlations over three bonds to the Q9 and Q10 carbonyl carbons. These carbons were correspondingly assigned from their HMBC correlations to Q1-CH and Q4-CH over three bonds. Finally, the Q6-CH and Q7-CH protons were assigned by decoupling the Q5-CH or the Q8-CH proton when the vicinal proton was observed as a doublet of doublets instead of a deceptive doublet of triplets.

In the phorbin part of the molecules, all protons except the 13^2-CH_2 protons showed one or several ROESY correlations to spatially adjacent groups. After one of the phorbin protons had been identified, its close neighbor protons could be tentatively assigned on the basis of the observed ROESY correlations. The most easily recognizable signals were given by the vinyl 3^1-CH, 3^2-CH_{trans} and 3^2-CH_{cis} protons, which exhibited their typical couplings and chemical shifts in all of the ^{1}H NMR spectra. However, the protons of the propionic 17^1-CH_2 and 17^2-CH_2 groups could be unambiguously assigned only after the spectral simulation of the propionic ester side-chain. The 13^2-CH_2 protons gave an AB-type spectrum, because these methylene protons are diastereotopic. The signal at higher δ_H value was assigned to H_A and that at lower δ_H value of H_B. After the molecular models (see Fig. 6) had been constructed, it became clear that the H_B proton is located below the phorbin macrocycle. This could be seen from the shielding effect on the 13^2-H_B by the ring current of the nearby quinone ring. Also, the signals arising from another pair of diastereotopic protons, the H_A and H_B of the phytyl P1-CH_2 group, were assigned by the corresponding method.

After the proton spectra had been assigned, the assignments of the ^{13}C NMR spectra were achieved easily using the numerous strong HMQC and HMBC correlations. In the ZnPQ2 and ZnP spectra, there were better separations between the ^{13}C resonances than in the ZnPQ1 and Q spectra. In spite of this variation, complete assignments could be deduced for the ^{13}C NMR spectra of all compounds studied.

Although the ^{13}C signals are known to be less sensitive to environmental alterations, some interesting differences could be seen between the P4 epimers. The anthraquinonyl carbon signals in ZnPQ1 and ZnPQ2 were shifted by *ca.* 2 ppm to higher field, except the Q9 carbon signal in ZnPQ1, which was shifted by 0.49 ppm to lower field relative to Q. A likely explanation for this is the coordination of the Q9 carbonyl oxygen to the central Zn(II) atom. This coordination is expected to withdraw electron density from the double bond between the Q9 carbon and oxygen, which would result in deshielding of the Q9 carbon.

Determination of the mutual orientation of the anthraquinone and phorbin rings in ZnPQ1

In the conformational analysis of ZnPQ1 and ZnPQ2, the mutual orientations of the rings were deduced by combining the information from the ROESY correlations between the rings with that obtained from the $\Delta\delta_H$ values. Thereafter, the conformations of ring D, the propionic ester side chain and the front part of the phytyl chain were determined from the vicinal coupling constants of the relevant protons.

In the ROESY spectrum of ZnPQ1, several correlations between the anthraquinone and pyropheophytin protons could be observed (Fig. 2). Conformationally, the most informative correlation was that between the Q1-CH and 18^1-CH_3 protons, which proved that the anthraquinone ring was located on the same side of the phorbin macrocycle as the 18^1-CH_3 group. The mutual positions of the ring planes could be evaluated more exactly from the other existing proton–proton correlations, Q4-CH–12^1-CH_3, Q5-CH–8^2-CH_3 and Q7-CH–7^1-CH_3 (Fig. 2). The correlation between the Q1-CH and 18^1-CH_3 protons was the strongest interplanar correlation whereas the other observed connectivities were close to the detection limit. Regarding the phytyl and macrocyclic protons of the pheophytin, only one ROESY correlation could be observed, which resulted from the interaction between the P2-CH and 17-CH protons.

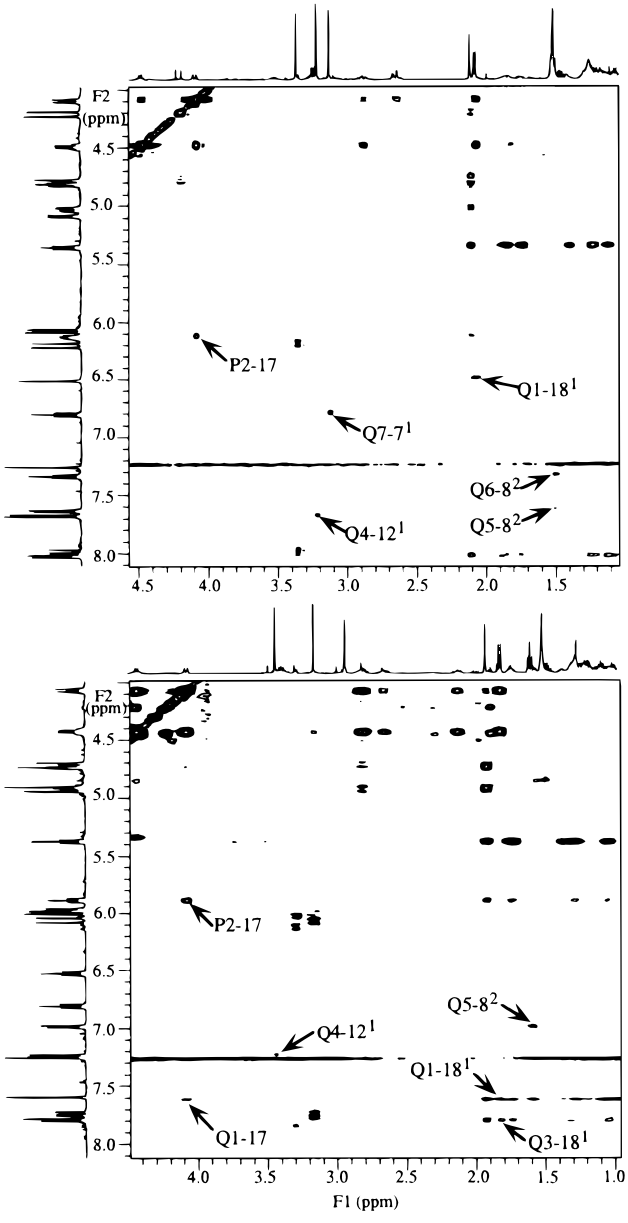

Figure 2. Conformationally informative parts of the ROESY spectra: top, ZnPQ1; bottom, ZnPQ2.

Geometric information can be obtained from the ring-current shifts, induced when two aromatic molecules are brought into a parallel geometry as a result of attractive π–π interactions between the π-systems.[27] Pheophytin aggregates have been extensively studied by constructing 'aggregation maps,' based on the $\Delta\delta_H$ values calculated by subtracting each δ_H value of the aggregate from the corresponding δ_H value of the monomer.[9,10] Similar principles have been applied to deduce the conformations of the metal-free derivatives, H_2PQ1 and H_2PQ2.[2] Here, the δ_H values of ZnPQ1 and ZnPQ2 were compared with the corresponding values of the standards ZnP and Q, and the $\Delta\delta_H$ values were obtained by subtraction. The mutual positions of the aromatic π-systems were determined by inspecting the $\Delta\delta_H$ values, which are attributable to the shielding ring-current effect of one π-system to the other one in the overlapping regions of the interacting rings.[9–13] The $\Delta\delta_H$ values obtained are assembled in the 'aggregation map' in Fig. 3. A small amount of pyrrolidine (5 equiv.) was added to prevent self-aggregation of ZnP in $CDCl_3$. Pyrrolidine is known to act as a fifth ligand in the case of Zn(II)–porphyrins and –pheophorbides.[5–7] The negative $\Delta\delta_H$ values imply upfield shifts (increased

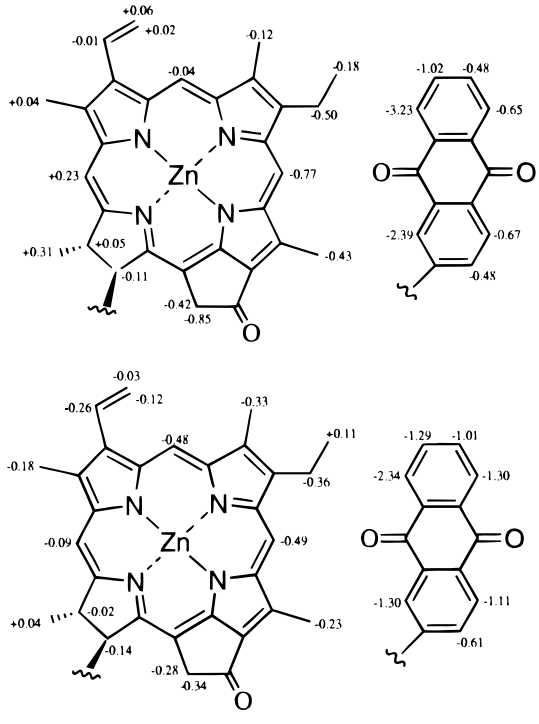

Figure 3. 'Aggregation maps' based on the $\Delta\delta_H$ values of the phorbin and anthraquinone rings: top, ZnPQ1; bottom, ZnPQ2. $\Delta\delta_H = \delta_H$ (ZnPQ1 or ZnPQ2) $- \delta_H$ (ZnP or Q).

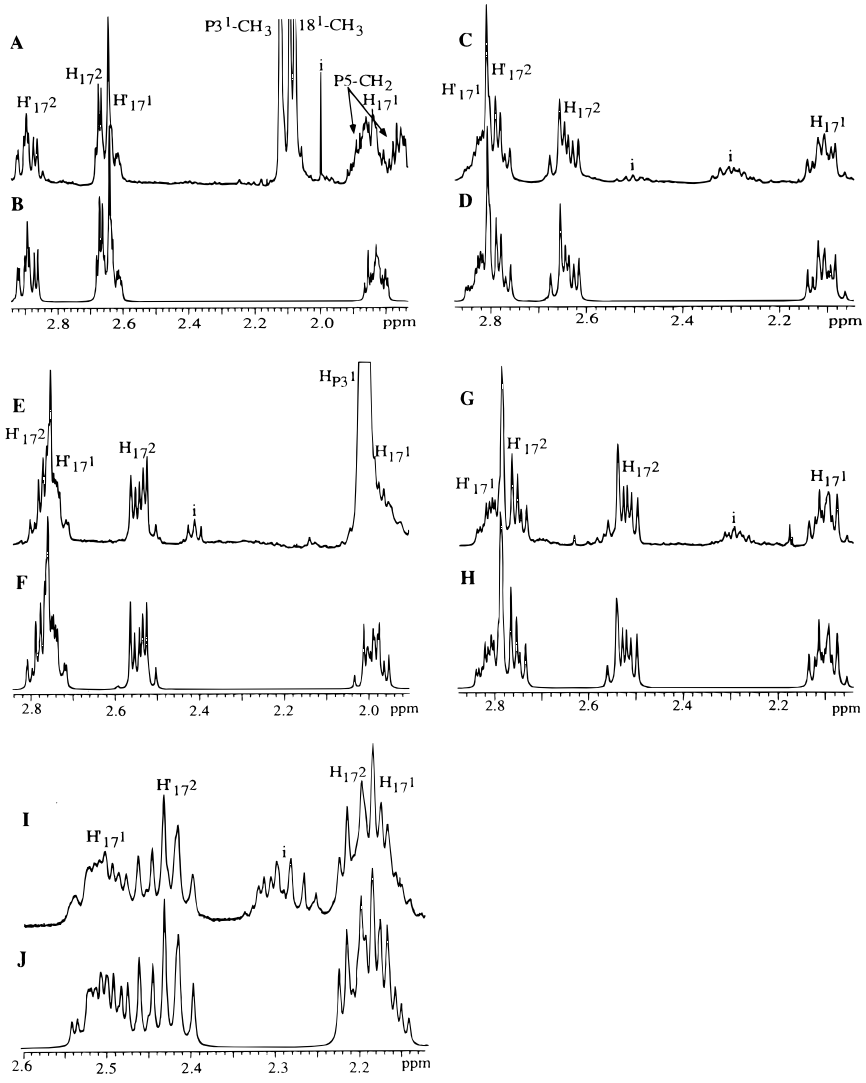

Figure 4. Observed (A, C, E, G, I) and simulated (B, D, F, H, J) spectra of the 17^1-CH_2 and 17^2-CH_2 protons of ZnPQ1 (A, B), ZnPQ2 (C, D), H_2PQ1 (E, F), H_2PQ2 (G, H) and ZnP (I, J); i = impurity.

shielding) whereas the positive $\Delta\delta_H$ values imply downfield shifts (deshielding).

In the phorbin part of ZnPQ1, the 18^1-CH_3 and 20-CH protons were clearly shifted downfield, whereas the 8^2-CH_2, 10-CH, 12^1-CH_3 and 13^2-CH_2 (H_B) protons were shifted upfield. In the anthraquinone part of ZnPQ1, the most shielded protons were Q1-CH (−2.39), Q7-CH (−1.02) and Q8-CH (−3.23) (δ, ppm). These are all on the left side of the quinone ring (Fig. 3). The strong shielding of these quinonyl protons (Fig. 3) implies their location inside the aromatic ring-current field of the Zn(II)–pyropheophytin ring. The shielding is much weaker for the right-side quinonyl protons and, hence, a longer distance to the phorbin ring-current field is expected for these protons. This implies either that the ring planes are in a tilted mutual orientation or that the overlapping of the rings is only partial (slipped parallel orientation). Both situations are possible, as can be seen from the constructed model of ZnPQ1 (see Fig. 6). The skew model of ZnPQ1 would explain the downfield shifts of the 18^1-CH_3 and 20-CH protons, as then these would be located in the deshielding zones of the anthraquinone Q9 and $Q2^1$ carbonyl groups.

Determination of the mutual orientations of the anthraquinone and phorbin rings in ZnPQ2

The ROESY spectrum of ZnPQ2 also exhibited several correlations between the anthraquinone and phorbin protons (Fig. 2). In addition, the strong correlation observed between the Q1-CH and 18^1-CH_3 protons shows that, also in this case, the quinone is located below the phorbin macrocycle. The other correlations observed between proton groups Q1-CH–17-CH, Q3-CH–18^1-CH_3, Q4-CH–12^1-CH_3, Q5-CH–8^2-CH_3 and Q8-CH–2^1-CH_3 (Fig. 2) provide further information of the relative orientation of the π-systems in ZnPQ2.

The phorbin protons were found to be mainly slightly shifted upfield in ZnPQ2. Inspection of the $\Delta\delta$ values in Fig. 3 shows that the shielding increment for protons 20-CH, 2^1-CH_3, 3^1-CH, 7^1-CH_3 and 8^2-CH_3 is in the range −0.10 to −0.17 ppm, with the exception of proton 5-CH, which is shielded by −0.42 ppm. The Q8-CH proton is clearly the most shielded quinone proton ($\Delta\delta_H = -2.34$), whereas shielding increases equally for the other quinone protons. These results can

be interpreted as indicating that the ring planes are in a parallel face-to-face geometry where the anthraquinone is located beneath the center of the phorbin macrocycle. The overall shielding pattern for the phorbin part of ZnPQ2 suggests that there may also be present some minor conformers where the quinone is located below the right edge of the phorbin ring.

Determination of the torsional angle in ring D of the derivatives

Conformational analysis of the pyropheophytin ring D, propionic ester side chain and front part of the phytyl chain was performed for ZnPQ1, ZnPQ2, their metal-free derivatives (H_2PQ1 and H_2PQ2) and reference compound ZnP. The torsional angle in ring D can be obtained from the vicinal coupling between the 17-CH and 18-CH protons. We used the simple Karplus equation,

$$^3J_{HH} = 10 \cos^2 \phi \quad (1)$$

to calculate the torsion angle ϕ.[25,26] The observed $^3J_{HH}$ couplings were 2.4, 2.0, 2.3, 1.8 and 2.8 Hz for ZnP, H_2PQ1, H_2PQ2, ZnPQ1 and ZnPQ2, respectively. Insertion of these couplings into the Karplus equation afforded ϕ values of 119°, 117°, 118°, 115° and 122°, respectively. Ring D is planar when the torsion angle of the vicinal protons is *ca.* 125°. A smaller torsion angle implies that C_{17} is located above and C_{18} below the phorbin ring plane.

Spectral simulations and rotamer population analysis

Spectral simulations of the proton signals arising from the propionic ester side chain and the front part of the phytyl chain (Fig. 4) give the $^3J_{HH}$ couplings, which can be used in the population analysis of the C_{17^1}–C_{17}, C_{17^2}–C_{17^1} and C_{P2}–C_{P1} rotamers (Fig. 5).[18,21–24] The propionic ester side chain protons were analyzed as an ABCDX (X = H_{17}) spin system. Figure 4 shows the observed and simulated spectra of the 17^1-CH_2 and 17^2-CH_2 protons of the dyads and ZnP. The model couplings for the propionic ester side chain protons (see Table 3) were obtained from a cyclohexane fragment with similar substituents using the approach of Feeney[28] or the simple Karplus equation [Eqn (1)].[21] The 17^1-CH_2 and 17^2-CH_2 protons were assigned with the aid of rotamers **1a**–**2c** (Fig. 5) assuming that the vicinal protons in *trans* (*t*) positions are coupled more strongly than those in *gauche* (*g*) positions. Of the geminal 17^1-CH_2 protons, that possessing a greater coupling constant to H_{17} was denoted H_{17^1} (*trans* to H_{17}, **1a**). In the case of the dyads, there is only one strong coupling between the 17^2-CH_2 protons and the H'_{17^1} proton, which indicates favor of the **2b** rotamer. Of the geminal 17^2-CH_2 protons, that with a greater coupling constant to H'_{17^1} was denoted H'_{17^2} (*trans* to H'_{17^1}, **2b**). In ZnP, there were two strong vicinal couplings between the 17^1-CH_2 and 17^2-CH_2 protons, indicating that these couplings arise from rotamer **2a**. In this case, the geminal 17^2-CH_2 protons were defined so that the one with a greater coupling constant to H'_{17^1} was denoted H_{17^2}. The calculated chemical shifts and couplings are presented in Table 1.

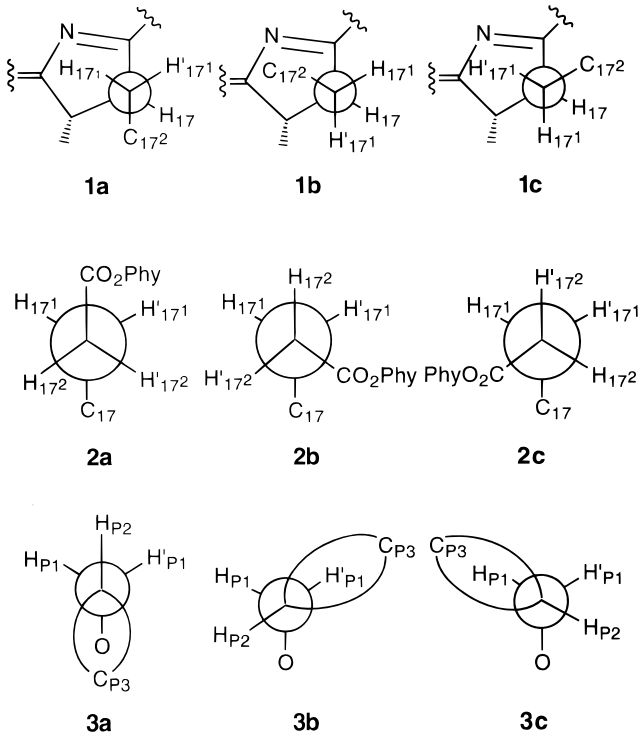

Figure 5. Staggered rotamers of the propionic ester side chain and the front part of the phytyl group in ZnP, H_2PQ1, H_2PQ2, ZnPQ1 and ZnPQ2.

The populations p_I, p_{II} and p_{III} (=1 − p_I − p_{II}) (Table 2) were calculated from the equations[33]

$$J_{AC\,(or\,BD)} = p_I J_t + p_{II} J_{g+} + (1 - p_I - p_{II}) J_{g-} \quad (2)$$

$$J_{BC\,(or\,AD)} = p_I J_{g+} + p_{II} J_t + (1 - p_I - p_{II}) J_{g-} \quad (3)$$

where J_{AC}, J_{BC}, J_{BD} and J_{AD} are the vicinal couplings obtained from the spectral simulations, and J_t, J_{g+} and J_{g-} are the model compound couplings shown in Table 3. For all compounds concerned, **1a** was the most populated C_{17^1}–C_{17}bond rotamer (Fig. 5). In the case of ZnPQ1 and ZnPQ2, **1a** was the only populated rotamer whereas for their metal-free derivatives **1b** was also slightly populated (p = 0.1). In the case of the quinone-free molecule ZnP, the population of rotamer **1b** increased to 0.3 at the expense of that of rotamer **1a** (p = 0.7). In the calculated populations, there was no observation of a contribution by the **1c** rotamer where the propionic chain is oriented towards ring E. Concerning the C_{17^2}–C_{17^1} bond rotamers, calculations showed that all rotamers **2a**–**c** were populated (Table 2). In ZnPQ1, rotamer **2b** was the most favored with p = 0.87. In the case of ZnPQ2, this rotamer was less populated but still the most favored one with p = 0.60. Also in the metal-free dyads, rotamer **2b** was clearly the most populated. In the H_2PQ and ZnPQ molecules, there was a balance between conformers **2b** (p = 0.57–0.80) and **2a** (p = 0.09–0.30). The populations of **2c** were equally small for all of the molecules (p = 0.11–0.13). In ZnP, rotamer **2a** was the most populated with p = 0.59 while the calculated population of rotamer **2b** was 0.29. Total inspection of the propionic side chain populations showed that ZnPQ1 has the most rigid structure and

Table 1 ^{1}H chemical shifts and simulated ^{1}H–^{1}H couplings of the propionic ester side chain and the front part of the phytyl-chain for ZnP, H_2PQ1, H_2PQ2, ZnPQ1 and ZnPQ2

	Chemical shift (ppm)						$^nJ_{HH}$ (n = 2 or 3) (Hz)				
Proton	ZnP	H_2PQ1	H_2PQ2	ZnPQ1	ZnPQ2	Coupling	ZnP	H_2PQ1	H_2PQ2	ZnPQ1	ZnPQ2
H_{17}	4.14	4.10	4.18	4.09	4.06	H_{17}–H_{17^1}	8.77	10.86	10.71	11.90	11.10
H_{17^1}	2.17	1.96	2.07	1.83	2.10	H_{17}–H'_{17^1}	3.21	2.26	2.96	2.70	2.68
H'_{17^1}	2.50	2.72	2.77	2.63	2.81	H_{17^1}–H'_{17^1}	−13.67	−13.86	−14.18	−14.04	−13.86
H_{17^2}	2.19	2.51	2.49	2.65	2.64	H_{17^1}–H_{17^2}	5.06	4.61	5.09	4.59	5.10
H'_{17^2}	2.43	2.74	2.73	2.89	2.79	H_{17^1}–H'_{17^2}	9.15	6.17	6.06	4.45	6.42
						H'_{17^1}–H_{17^2}	9.45	6.69	6.88	4.48	6.19
						H'_{17^1}–H'_{17^2}	6.88	9.79	9.65	11.31	10.23
						H_{17^2}–H'_{17^2}	−15.74	−15.61	−15.60	−15.20	−15.18
H_{P1}	4.29	4.85	4.88	5.02	4.91	H_{P1}–H_{P2}	7.35	6.22	6.99	5.78	6.87
H'_{P1}	4.27	4.75	4.70	4.80	4.72	H'_{P1}–H_{P2}	6.88	8.45	6.79	9.74	7.01
H_{P2}	5.09	5.93	5.90	6.12	5.88	H_{P1}–H'_{P1}	−12.20	−12.54	−12.67	−12.25	−12.61

that ZnPQ2 is more rigid than its metal-free derivative. It is also noticeable that the most populated C_{17^1}–C_{17} and C_{17^2}–C_{17^1} bond rotamers are the same in all dyads studied.

Table 2 Calculated populations of the propionic ester side chain of ZnP, H_2PQ1, H_2PQ2, ZnPQ1 and ZnPQ2

		Calculated populations				
	Rotamer	ZnP	H_2PQ1	H_2PQ2	ZnPQ1	ZnPQ2
C_{17^1}–C_{17}	**1a**	0.7	0.9	0.9	1.0	1.0
	1b	0.3	0.1	0.1	0.0	0.0
	1c	0.0	0.0	0.0	0.0	0.0
C_{17^2}–C_{17^1}	**2a**	0.59	0.29	0.30	0.09	0.28
	2b	0.29	0.60	0.57	0.80	0.61
	2c	0.12	0.11	0.13	0.11	0.11
C_{P2}–C_{P1}	**3a**	0.01	−0.04	0.06	−0.14	0.07
	3b[a]	0.47	0.65	0.48	0.80	0.47
	3c[a]	0.52	0.39	0.46	0.34	0.46

[a] These populations are interchangeable owing to the missing P1-CH_2 proton assignments.

Table 3 Model compound couplings for rotamers 1a–3c[21–23]

	$^3J_{HH}$		
Coupled protons	**1a**	**1b**	**1c**
H_{17}–H_{17^1}	11.5	3.0	3.0
H_{17}–H'_{17^1}	3.0	3.0	11.5
	2a	**2b**[a]	**2c**[a]
H'_{17^1}–H'_{17^2}	4.4	13.2	2.8
H_{17^1}–H'_{17^2}	13.2	3.6	3.6
H'_{17^1}–H_{17^2}	13.2	3.6	3.6
H_{17^1}–H_{17^2}	4.4	2.8	13.2
	3a	**3b**	**3c**
H_{P2}–H'_{P1}	2.8	2.8	11.5
H_{P2}–H_{P1}	2.8	11.5	2.8

[a] Revised coupling values (compare with our previous values in Table 2 in Ref. 18).

In the front part of the phytyl chain, the P1-CH_2 and P2-CH protons generate a simple three-spin ABK system which was also simulated in order to separate overlapping signals in the spectra. The conformer populations of this fragment could be determined in the same way as mentioned above by applying model compound couplings.[18] Using allyl methyl ether as the model compound, the phytyl front part can exist in conformations **3a–c** (Fig. 5).[23] The corresponding coupling values are presented in Table 3. For the H_A and H_B protons of P1-CH_2, no absolute assignments could be made, hence the populations obtained are interchangeable. However, in the case of Zn(II) dyads, the conclusions drawn from ROESY and molecular models show that the P3^1-methyl group is oriented away from macrocyclic planes in favor of rotamer **3b**. For ZnP, H_2PQ2 and ZnPQ2, the **3b** and **3c** conformers are almost equally populated and the population of the **3a** rotamer is close to zero. The populations obtained for the **3a–c** rotamers of H_2PQ1 and ZnPQ1 raise a question about the validity of the model couplings used in our case, as the insertion of the measured coupling values into Eqns (2) and (3) yielded negative **3a** populations for H_2PQ1 ($p = -0.04$) and ZnPQ1 ($p = -0.14$) (Table 2). The reason for the negative population might arise from the rigidity of the Zn(II)–pyropheophytin–anthraquinone structure, which is expected to restrict rotations in the front part of the phytyl chain and to cause deviations from the model compound conformers (**3a–c**).

Molecular modeling

Molecular modeling was used to construct the folded conformers of the ZnPQ1 and ZnPQ2 (Fig. 6). The conformers were constructed first on the basis of the information given by ROESY and the vicinal proton–proton couplings and, thereafter, the structures were optimized in the MM+ force-field. The mutual positions of the rings could be constructed explicitly using the ROESY correlations and analyzing the $\Delta\delta_H$ values. The only contradiction in the constructed structures is the existence of ROESY correlations between Q1-CH–18^1-CH_3, Q3-CH–18^1-CH_3 and Q1-CH–17-CH in ZnPQ2. According to molecular modeling, the Q3-CH–18^1-CH_3

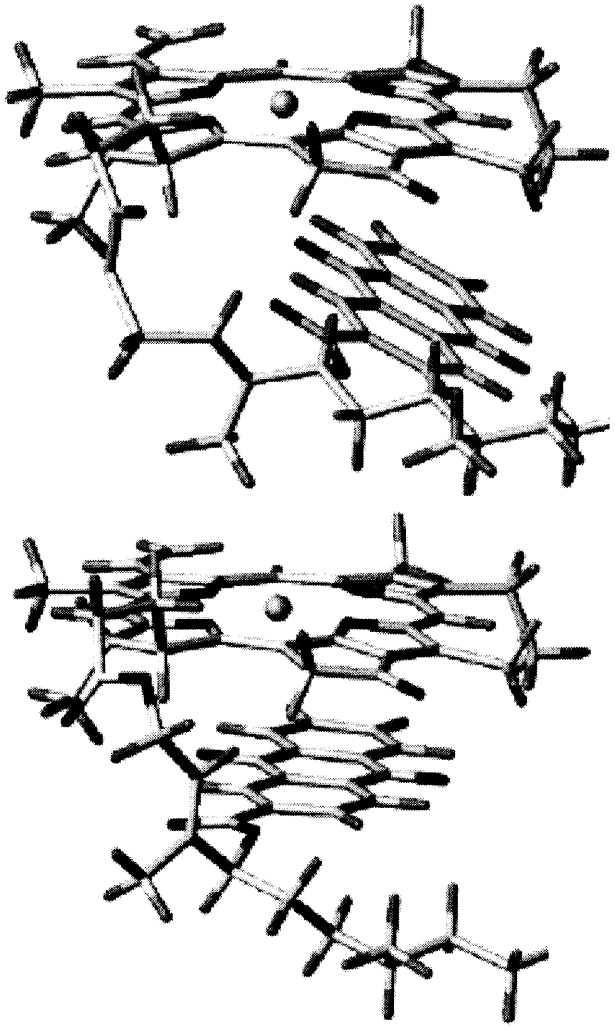

Figure 6. Structures of the optimized molecular models: top, ZnPQ1; bottom, ZnPQ2. The phytyl side chain has been cut off from the P6 carbon.

and Q1-CH–17-CH proton correlations cannot both exist in the same conformer. A reasonable explanation for this contradiction is a relatively long mixing time (800 ms), which allows spin diffusion between scalar coupled protons. This may cause 'false' ROESY correlations that arise during the spin-lock period when it is developed by a DANTE-type pulse sequence.[29,30] Proton Q1-CH is coupled to Q3-CH with 1.6 Hz, which allows the spin diffusion between these protons. When a set of shorter mixing times is used, the correlation between Q1-CH–18^1-CH_3 grows up before the rise of the Q3-CH–18^1-CH_3 correlation. However, the use of a relatively long mixing time also allowed the observation of several clear real ROESY correlations. This phenomenon could explain the observed correlations that are highly improbable for a single conformer. Taking into account the other ROESY correlations in ZnPQ2, we have constructed a model where the Q3-CH–18^1-CH_3 correlation was less probable than the Q1-CH–18^1-CH_3 correlation (Fig. 6).

In the computational structure optimization, the torsion angle between the H_{17}–H_{18} protons was constrained but the other structural parameters were optimized freely. The convergence energy was 130 kcal mol^{-1} (1 kcal = 4.184 kJ) for both model structures shown in Fig. 6. These structures are in agreement with the NMR information. The minimized energy of the opened conformers, where the phorbin and anthraquinone rings were far apart from each other, was *ca.* 15 kcal mol^{-1} higher than that for the folded conformers. In solution, the energy differences are probably lower owing to solvent stabilization. In addition, it should be noted that the MM+ force field is not optimized to situations involving π–π or Zn(II) coordination interactions. Therefore, the molecular modeled structures are presented here mainly to help structural visualization of the NMR results.

On the basis of the ROESY spectra, no direct indication of the stereochemistry at C-P4 could be achieved. Nevertheless, the comparison of the dihedral angles of ring D in ZnP, ZnPQ1 and ZnPQ2 made it possible to assign the C-P4 configurations in the dyad epimers. In the case of the P4(*S*) epimer, the anthraquinone ester bridge is oriented upwards from C-P4, thereby forcing the C-17 carbon down. In that situation an increase in the dihedral angle between H_{17} and H_{18} is expected relative to ZnP. In the P4(*R*) epimer the reverse behavior of the H_{17}–H_{18} dihedral angle is expected, as the anthraquinone ester bridge is now oriented downwards from C-P4. Comparison of the H_{17}–H_{18} ϕ values in the P4 epimers of ZnPQ1 and ZnPQ2 with the corresponding ϕ value of ZnP shows that, in ZnPQ1, the angle is decreased by 3°, whereas in ZnPQ2 it is increased by 4°. These results suggest reconsideration of our previous proposal[2] for the P4 configurations in H_2PQ1 and H_2PQ2 (or ZnPQ1 and ZnPQ2). On the basis of the evidence now obtained, it seems likely that the P4(*R*) configuration belongs to H_2PQ1/ZnPQ1 and the P4(*S*) configuration to H_2PQ2/ZnPQ2 (Fig. 1). These assignments are in accordance with the finding that in the ZnPQ2 epimer, the anthraquinone ring is located in a more parallel and more centered position beneath the phorbin macrocycle, whereas in the ZnPQ1 epimer, the anthraquinone ring is situated in a sloping orientation below the phorbin subrings B, C and E owing to the coordination interaction between the quinone carbonyl oxygen and the central Zn(II) atom (Fig. 6).

CONCLUSIONS

In the folded conformers of the metal-free pyropheophytin–anthraquinone dyads, the estimated distance between the phorbin and anthraquinone planes exceeds 5–7 Å.[2] In the folded conformers of the Zn(II) dyads, the interplanar distance is shortened to the ROESY distance, which we estimate to be *ca.* 4 Å. The coordination of the anthraquinone carbonyl to the central Zn atom and the π–π interactions between the π-systems can be considered as driving forces for the formation of the folded conformers of the Zn(II)–phorbin–anthraquinone dyads. Apparently, the combination of these forces is more optimal in the case of ZnPQ1, thus making its structure more rigid than that of ZnPQ2. In ZnPQ2, there is more motional freedom in the propionic acid residue part and the front part of the phytyl chain than in ZnPQ1. The higher

internal mobility of ZnPQ2 can be inferred from the results showing that rotamers **1a**–**3c** are more equally populated in ZnPQ2 than in ZnPQ1. In the structure deduced for the folded conformer of ZnPQ1 (Fig. 6), the Q9 carbonyl oxygen is in the proximity of the central zinc atom and the rings show tilting. Therefore, it seems likely that in the ZnPQ1 structure, the anthraquinone carbonyl oxygen is coordinated to the central zinc atom.

To obtain the required information for the construction of the molecular models, several NMR techniques were needed. The rotamer populations calculated from the vicinal proton–proton couplings indicate that the structures obtained are relatively mobile. It should be noted that the final structures obtained represent the average conformations for the Zn(II) dyads in $CDCl_3$. As the proton chemical shifts are very sensitive to the alterations in the surroundings, the analysis of the $\Delta\delta_H$ values is still a useful method despite the fact that an unambiguous interpretation of these values is more difficult than the interpretation of ROESY information. To understand better the nature of the driving forces concerned in the formation of the folded conformers, additional NMR investigation should be carried out paying attention to dynamic and environmental factors such as temperature and solvent effects.

EXPERIMENTAL

The syntheses of ZnP, H_2PQ1, H_2PQ2, ZnPQ1 and ZnPQ2 have been described in a previous paper.[2] The NMR samples were prepared by dissolving 30 mg of Q, 7 mg of ZnPQ1, 9 mg of ZnPQ2 or 10 mg of ZnP in 0.6 ml of $CDCl_3$ (Aldrich, 99.5% D) in a 5 mm NMR tube. A small amount of tetramethylsilane (TMS) was added to the solution as an internal standard (0.00 ppm). All 2D spectra were recorded at 300 K (27 °C), non-spinning, on a Varian Unity 500 NMR spectrometer. In the ROESY measurements, mixing times of 100–800 ms and a relaxation delay of 1.5 s were used. The spin-lock field was generated using a DANTE-type pulse sequence. The spectral width in F_1 and F_2 was set to 5 kHz. The number of transients was 32 and 256 time increments were collected using the hypercomplex method. The acquired 2 × 1K × 256 data matrix was zero-filled to give a 2 × 2K × 1K matrix and processed using $\pi/2$ shifted sine-bell filter functions in both domains prior to Fourier transformation (FT). The detailed measuring conditions for HMQC and HMBC spectra have been described previously.[16] In the HMQC and HMBC experiments, the spectral width was set to 5 kHz in F_2 and to 26 kHz in F_1. The relaxation delay between transients was 1.1 s. In the HMQC measurements, the number of transients was 64 and 288 time increments were acquired. The data were zero-filled to give a 2 × 4K × 1K data matrix prior to FT. In the HMBC measurements, the number of transients was 96 and 272 time increments were collected. The data was zero-filled to give a 2 × 4K × 1K data matrix. All data in the 2D experiments were collected using the hypercomplex method.

Spectral simulations

The computer simulations of the ^{1}H NMR spectra were performed using LAOCOON-3 type MDL analysis[31] and PERCH software.[32] For the propionic part of the C-17 side chain, the number of spectral parameters to be iterated was 13. In the simulated spectra of ZnP, H_2PQ1, H_2PQ2, ZnPQ1 and ZnPQ2, there were 94, 90, 86, 91 and 89 computed transitions, of which 78, 66, 69, 59 and 74 were assigned, respectively. The number of observed peaks was 37, 30, 38, 33 and 34. The obtained r.m.s. values were 0.17, 0.22, 0.14, 0.32 and 0.19 Hz and the largest deviations were 0.25, 0.24, 0.11, 0.40 and 0.14 Hz. In the simulation of the phytyl P1-CH_2 and P2-CH spectra, the number of spectral parameters to be iterated was six. The number of observed peaks was 11, and there were 12 computed transitions which were all assigned. The precision was high in every phytyl spectrum simulation, but the r.m.s. and the largest deviations could not be obtained because of the strong correlation between the simulation parameters. The simulation accuracy for the propionic part is acceptable owing to a large natural linewidth (1.8–2.2 Hz). In the cases of H_2PQ1 and ZnPQ1, the overlapping between the 13^2-CH_B and P1-H_B (H_{BP1} in Table 1) proton signals caused a decrease in the accuracy.

Molecular modeling

The computer-aided molecular modelings were performed on a 486 PC computer using the MM+ molecular mechanic force-field and the HyperChem program (software 4.5) (Hypercube, Waterloo, ON, Canada). The atom types for the MM+ force-field were determined utilizing the HyperChem calculation option. Structures were energy optimized in terms of the dipole bond parameter calculation using the Newton–Raphson optimization algorithm with an energy convergence criterion of 0.01 kcal mol^{-1} $Å^{-1}$.

^{1}H and ^{13}C NMR spectra of Q

^{1}H NMR ($CDCl_3$), δ_H (ppm) 8.90 (dd, 1 H, 1.7, 0.5 Hz, Q1), 8.40 (dd, 1 H, 8.1, 1.7 Hz, Q3), 8.35 (dd, 1 H, 8.1, 0.5 Hz, Q4), 8.31 (m, 1 H, Q8), 8.29 (m, 1 H, Q5), 7.82 (m, 2 H, Q6, Q7), 4.01 (s, 3 H, $Q2^2$); ^{13}C NMR (δ in $CDCl_3$), δ_C (ppm) 182.46 (Q10), 182.18 (Q9), 165.46 ($Q2^1$), 136.05 (Q12), 135.13 (Q11)[a], 134.50 (Q3), 134.45 (Q5)[b], 134.37 (Q6)[b], 133.53 (Q14)[a], 133.42 (Q13)[a], 133.34 (Q2)[a], 128.60 (Q1), 127.54 (Q4), 127.43 (Q7)[c], 127.38 (Q8)[c], 52.75 ($Q2^2$) (see end of text for meaning of superscript letters).

^{1}H and ^{13}C NMR spectra of ZnP

^{1}H NMR ($CDCl_3$ with 5 eqiv. of pyrrolidine relative to ZnP), δ_H (ppm) 9.49, 9.24, 8.31 (singlets, 1H, 10, 5, 20), 8.01 (dd, 1 H, 17.8, 11.5 Hz, 3^1), 6.18 (dd, 1 H, 17.8, 1.5 Hz, 3^2, H_{trans}), 6.02 (dd, 1 H, 11.5, 1.5 Hz, 3^2, H_{cis}), 5.23

(t, 1 H, 7.1 Hz, P2), 5.21, 5.06 (dd, 1 H, 19.4 Hz, 13^2, H_A, H_B), 4.53 (d, 2 H, 7.1 Hz, P1), 4.44 (qd, 1 H, 7.4, 2.4 Hz, 18), 4.21 (m, 1 H, 17), 3.75 (q, 2 H, 7.7 Hz, 8^1), 3.66 (s, 3 H, 12^1), 3.33 (s, 3 H, 2^1) 3.26 (s, 3 H, 7^1), 2.70–2.25 (m, 4 H, 17^1 and 17^2 in Table 2), 1.77 (d, 3 H, 7.3 Hz, 18^1), 1.70 (t, 3 H, 7.6 Hz, 8^2), 1.63 (s, 3 H, P3^1); ^{13}C NMR (δ in $CDCl_3$), δ_C (ppm) 196.57 (13^1), 172.94 (17^3), 168.35 (19), 161.11 (14), 156.21 (16), 153.81 (1), 150.73 (6), 147.16 (11)[d], 146.93 (4)[d], 144.68 (9), 143.62 (8), 142.95 (P3), 138.98 (3), 134.63 (2), 134.32 (12), 133.20 (7), 131.48 (13), 129.97 (3^1), 120.84 (3^2), 117.63 (P2), 106.31 (10), 105.33 (15), 99.03 (5), 92.40 (20), 61.47 (P1), 50.55 (17), 48.62 (18), 47.83 (15^2), 47.83 (13^2), 39.75 (P4), 30.90 (17^2), 29.36 (17^1), 23.48 (18^1), 19.21 (8^1), 17.28 (8^2), 16.29 (P3^1), 12.45 (12^1), 12.28 (2^1), 10.71 (7^1).

^{1}H and ^{13}C NMR spectra of ZnPQ1

^{1}H NMR ($CDCl_3$), δ_H (ppm) 9.20, 8.72, 8.54 (singlets, 1 H, 5, 10, 20), 8.03 (dd, 1 H, 7.9, 1.6 Hz, Q3), 8.00 (dd, 1 H, 17.8, 11.5 Hz, 3^1), 7.68 (d, 1 H, 7.9 Hz, Q4), 7.64 (br. d, 1 H, 7.6 Hz, Q5), 7.34 (td, 1 H, 7.6, 1.1 Hz, Q6), 6.80 (td, 1 H, 7.6, 1.1 Hz, Q7), 6.51 (br. d, 1 H, 1.6 Hz, Q1), 6.20 (dd, 1 H, 17.8, 1.5 Hz, 3^2, H_{trans}), 6.13 (m, 2 H, P2), 6.08 (dd, 1 H, 11.4, 1.5 Hz, 3^2, H_{trans}), 5.35 (br. t, 1 H, 6.6 Hz, P4), 5.08 (br. d, 1H, 7.6 Hz, Q8), 5.05–4.75 (m, 2 H, P1, H_A and H_B in Table 2), 4.79 (d, 1 H, 19.5 Hz, 13^2, H_A), 4.49 (qd, 1 H, 7.4, 1.8 Hz, 18), 4.21 (d, 1 H, 19.5 Hz, 13^2, H_B), 4.10 (m, 1 H, 17), 3.37 (s, 3 H, 2^1), 3.25 (q, 2 H, 7.4 Hz, 8^1), 3.23 (s, 3 H, 12^1), 3.14 (s, 3 H, 7^1), 2.95–1.80 (m, 4 H, 17^1 and 17^2 in Table 2), 2.12 (br. s, 3 H, P3^1), 2.08 (d, 3 H, 7.4 Hz, 18^1); ^{13}C NMR (δ in $CDCl_3$), δ_C (ppm) 195.86 (13^1), 182.67 (Q9), 180.98 (Q10), 172.66 (17^3), 168.97, (19), 163.61 ($Q2^1$), 160.98 (14), 158.02 (16), 153.90 (2), 150.67 (6), 147.58 (4), 146.16 (11), 144.64 (9), 143.43 (8), 139.47 (P3), 138.98 (3), 135.07 (2), 134.15 (Q12), 133.78 (12)[e], 133.49 (Q3)[e], 133.28 ($Q11^f$, Q6)[e], 133.12 (7), 132.31 (Q7), 131.72 (Q14), 130.73 (13)[g], 130.50 ($Q2^f$, Q13)[g], 130.17 (3^1), 127.62 (Q1), 126.10 (Q4), 125.65 (Q5, Q8), 124.30 (P2), 120.72 (3^2), 105.93 (10), 105.08 (15), 98.74 (5), 93.04 (20), 81.26 (P4), 60.39 (P1), 49.79 (17), 49.12 (18), 47.77 (13^2), 32.05 (17^2), 30.64 (17^1), 23.91 (18^1), 19.24 (8^1), 17.33 (8^2), 12.42 (2^1), 12.04 (12^1), 11.93 (P3^1), 10.80 (7^1).

^{1}H and ^{13}C NMR spectra of ZnPQ2

^{1}H NMR ($CDCl_3$), δ_H (ppm) 9.00, 8.76, 8.22 (s, 1 H, 10, 5, 20), 7.79 (dd, 1 H, 8.0, 1.6 Hz, Q3), 7.75 (dd, 1 H, 17.8, 11.4 Hz, 3^1), 7.60 (br. d, 1 H, 1.6 Hz, Q1), 7.24 (d, 1 H, 8.0 Hz, Q4), 6.99 (br. d, 1 H, 7.5 Hz, Q5), 6.81, 6.53 (br. t, 1 H, Q6, Q7), 6.06 (dd, 1 H, 17.8, 1.5 Hz, 3^2, H_{trans}), 5.99 (dd, 1 H, 11.4, 1.5 Hz, 3^2, H_{cis}), 5.89 (br. t, 1 H, 7.0 Hz, P2), 5.38 (t, 1 H, 6.7 Hz, P4), 4.93 (d, 1 H, 19.4 Hz, 13^2, H_A), 4.95–4.70 (m, 2 H, P1, H_A and H_B in Table 2), 4.72 (d, 1 H, 19.4 Hz, 13^2, H_B), 4.42 (qd, 1 H, 7.4, 2.8 Hz, 18), 4.07 (m, 1 H, 17), 3.43 (s, 3 H, 12^1), 3.39 (q, 2 H, 7.6 Hz, 8^1), 3.15 (s, 3 H, 2^1), 2.93 (s, 3 H, 7^1), 2.85–2.00 (m, 4 H, 17^1 and 17^2 in Table 2), 1.91 (s, 3 H, P3^1), 1.81 (d, 3 H, 7.4 Hz, 18^1), 1.59 (t, 3 H, 7.6 Hz, 8^2); ^{13}C NMR (δ in $CDCl_3$), δ_C (ppm) 196.15 (13^1), 180.33 (Q10), 179.95 (Q9), 172.80 (17^3), 167.93 (19), 163.40 ($Q2^1$), 160.84 (14), 156.72 (16), 153.12 (1), 150.03 (6), 146.67 (11)[h], 146.61 (4)[h], 144.43 (9), 143.33 (8), 139.57 (P3), 138.30 (3), 134.33 (2), 134.20 (12, $Q11^i$, Q12), 133.57 (Q3), 132.79 (7), 132.57 (Q6, Q7), 131.42 (13, $Q2^i$), 130.99 (Q14), 130.72 (Q13), 129.86 (3^1), 127.15 (Q1), 126.19 (Q4), 125.63 (Q5), 125.10 (Q8), 121.81 (P2), 120.46 (3^2), 106.14 (10), 105.32 (15), 98.52 (5), 92.16 (20), 79.83 (P4), 60.68 (P1), 50.40 (17), 48.66 (18), 48.06 (13^2), 31.97 (17^2), 30.29 (17^1), 23.41 (18^1), 19.10 (8^1), 17.31 (8^2), 13.35 (P3^1), 12.46 (12^1), 12.18 (2^1), 10.54 (7^1).

Mutually similar superscript letters indicate which ^{13}C NMR resonances are mutually interchangeable, as the differences of the chemical shifts are at the limits of experimental HMQC and HMBC resolutions.

REFERENCES

1. A. Y. Tauber, J. Helaja, N. V. Tkachenko, H. Lemmetyinen, I. Kilpeläinen and P. H. Hynninen, in *Photosynthesis: from Light to Biosphere*, edited by P. Mathis, Vol. VI, p. 815. Kluwer, Dordrecht (1995).
2. A. Y. Tauber, R. K. Kostiainen and P. H. Hynninen, *Tetrahedron* **50**, 4723 (1994).
3. D. Gust, T. A. Moore, P. A. Liddell, G. A. Nemeth, L. R. Makings, A. L. Moore, D. Barrett, P. J. Pessiki, R. V. Bensasson, M. Rougée, C. Chanchaty, F. C. De Schryver, M. Van der Auweraer, A. R. Holzwarth and S. J. Connolly, *J. Am. Chem. Soc.* **109**, 846 (1987).
4. V. V. Borovkov, A. A. Gribkov, A. N. Kozyrev, A. S. Brandis, A. Ishida and Y. Sakata, *Bull. Chem. Soc. Jpn.* **65**, 1533 (1992).
5. R. J. Abraham, P. Leighton and J. K. M. Sanders, *J. Am. Chem. Soc.* **107**, 3472 (1985).
6. R. J. Abraham, G. R. Bedford and B. Wright, *Org. Magn. Reson.* **18**, 45 (1982).
7. R. J. Abraham, K. M. Smith, D. A. Goff and J.-J. Lai, *J. Am. Chem. Soc.* **104**, 4332 (1982).
8. G. M. Sanders, M. van Dijk, A. van Veldhuizen and H. C. van der Plas, *J. Chem. Soc., Chem. Commun.* 1311 (1986).
9. J. J. Katz, G. L. Closs, F. C. Pennington, M. R. Thomas and H. H. Strain, *J. Am. Chem. Soc.* **85**, 3801 (1963).
10. G. L. Closs, J. J. Katz, F. C. Pennington, M. R. Thomas and H. H. Strain, *J. Am. Chem. Soc.* **85**, 3809 (1963).
11. J. J. Katz, R. C. Dougherty and L. J. Boucher, in *The Chlorophylls*, edited by L. P. Vernon and G. R. Seely, p. 185. Academic Press, London (1966).
12. P. H. Hynninen and S. Lötjönen, *Biochim. Biophys. Acta* **1083**, 374 (1993).
13. H. Scheer and J. J. Katz, in *Porphyrins and Metalloporphyrins*, edited by K. M. Smith, p. 399. Elsevier, Amsterdam (1975).
14. R. J. Abraham and A. E. Rowan, in *Chlorophylls*, edited by H. Scheer, p. 797. CRC Press, Boca Raton, FL (1991).
15. C. A. Hunter and J. K. M. Sanders, *J. Am. Chem. Soc.* **112**, 5525 (1990).
16. I. Kilpeläinen, S. Kaltia, P. Kuronen, K. Hyvärinen and P. H. Hynninen, *Magn. Reson. Chem.* **32**, 29 (1994).
17. K. Hyvärinen, J. Helaja, P. Kuronen, I. Kilpeläinen and P. H. Hynninen, *Magn. Reson. Chem.* **33**, 646 (1995).
18. J. Helaja, K. Hyvärinen, S. Heikkinen, I. Kilpeläinen and P. H. Hynninen, *J. Mol. Struct.* **354**, 71 (1995).
19. M. F. Summers, L. G. Marzilli and A. Bax, *J. Am. Chem. Soc.* **109**, 566 (1987).
20. A. A. Bothner-By, R. L. Stephens, J. Lee, C. D. Warren and R. W. Jeanloz, *J. Am. Chem. Soc.* **106**, 811 (1984).
21. K. M. Smith, D. A. Goff and R. J. Abraham, *Tetrahedron Lett.* **22**, 4873 (1981).
22. K. M. Smith, D. A. Goff and R. J. Abraham, *J. Org. Chem.* **52**, 176 (1987).

23. K. M. Smith, D. A. Goff and R. J. Abraham, *Org. Magn. Reson.* **22**, 779 (1984).
24. S. Lötjönen, T. J. Michalski, J. R. Norris and P. H. Hynninen, *Magn. Reson. Chem.* **25**, 670 (1987).
25. M. Karplus, *J. Chem. Phys.* **30**, 11 (1959).
26. R. J. Abraham, J. Fisher and P. Loftus, *Introduction to NMR Spectroscopy*, 2nd edn, p. 34. Wiley, Chichester (1988).
27. H. Günther, *NMR Spectroscopy*, pp. 85 and 515. Wiley, Chichester (1995).
28. J. Feeney, *J. Magn. Reson.* **21**, 473 (1975).
29. D. Neuhaus and J. Keeler, *J. Magn. Reson.* **68**, 568 (1986).
30. D. Neuhaus and M. P. Williamson, *The Nuclear Overhauser Effect in Structural and Conformational Analysis*, p. 74. VCH, New York (1989).
31. R. J. Laatikainen, *J. Magn. Reson.* **92**, 1 (1991).
32. R. J. Laatikainen and M. Niemitz, *PERCH Project*. Department of Chemistry, University of Kuopio.
33. F. W. Wehrli, A. P. Marchand and S. Wehrli, *Interpretation of Carbon-13 NMR Spectra*, 2nd edn., p. 323, Wiley, Chichester (1988).

